A Simple Approach Toward Low-Dielectric Polyimide Nanocomposites: Blending the Polyimide Precursor with a Fluorinated Polyhedral Oligomeric Silsesquioxane

YUN-SHENG YE,[1] YING-CHIEH YEN,[1] WEN-YI CHEN,[2] CHIH-CHIA CHENG,[1] FENG-CHIH CHANG[1]

[1]Institute of Applied Chemistry, National Chiao Tung University, Hsinchu, Taiwan

[2]Material and Chemical Research Laboratories, Industrial Technology Research Institute, Chutung, Taiwan

Received 19 March 2008; accepted 18 June 2008
DOI: 10.1002/pola.22939
Published online in Wiley InterScience (www.interscience.wiley.com).

ABSTRACT: This article describes a new and simple method for preparing polyimide nanocomposites that have very low dielectric constants and good thermal properties: simply through blending the polyimide precursor with a fluorinated polyhedral oligomeric silsesquioxane derivative, octakis(dimethylsiloxyhexafluoropropyl) silsesquioxane (OF). The low polarizability of OF is compatible with polyimide matrices, such that it can improve the dispersion and free volume of the resulting composites. Together, the higher free volume and lower polarizability of OF are responsible for the lower dielectric constants of the PI-OF nanocomposites. This simple method for enhancing the properties of polyimides might have potential applicability in the electronics industry. © 2008 Wiley Periodicals, Inc. J Polym Sci Part A: Polym Chem 46: 6296–6304, 2008

Keywords: blending; dielectric properties; morphology; nanocomposites; polyimides

INTRODUCTION

Polyimides are important materials for microelectronics applications. A number of techniques have been explored for the synthesis of polyimides having low dielectric constant. Among them, fluorination is one of the most widely adapted techniques for reducing the dielectric constants of polyimides.[1–6] Another approach is the introduction of nanopores into the polyimides, because air has the lowest dielectric constant (ca.1).[7–9] Porous, low-dielectric-constant polyimides can be obtained by creating voids through the thermal degradation of labile blocks or grafts of polyimides. Unfortunately, these two approaches (fluorination and thermal degradation) usually result in polyimides exhibiting poor thermal and mechanical properties.[1,2,10] Thus, the development of more efficient methods for reducing the dielectric constant without detrimentally affecting the thermal and mechanical properties of polyimides remains an important goal.

Polyhedral oligomeric silsesquioxane (POSS) moieties possess nanometer-sized structures, high thermal stabilities, monodispersity, controlled porosity, and adjustable chemical functionality. They are important starting materials for the design of several hybrid nanostructure materials.[11–23] The miscibility between a polymer matrix and POSS substituents dictates the morphology and physical properties of the resulting polymer/

Additional Supporting Information may be found in the online version of this article.

Correspondence to: F.-C. Chang (E-mail: changfc@mail.nctu.edu.tw)

Journal of Polymer Science: Part A: Polymer Chemistry, Vol. 46, 6296–6304 (2008)

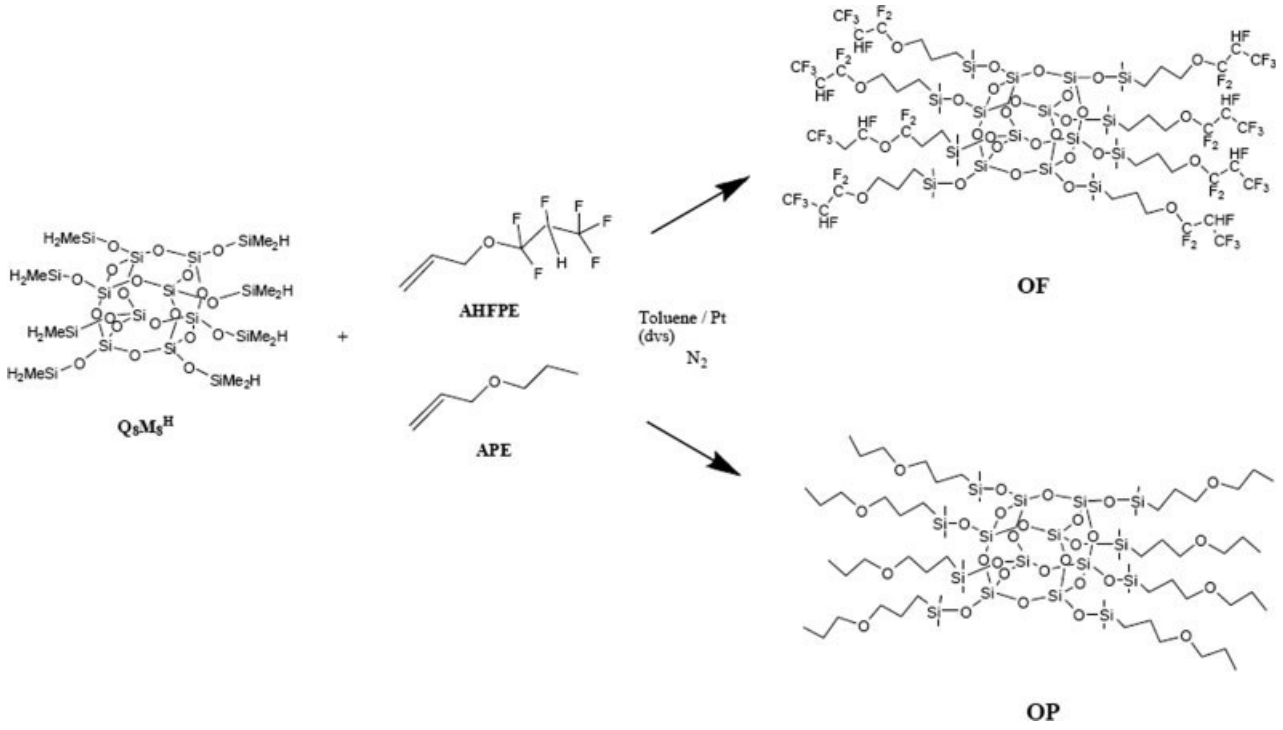

Scheme 1. Synthesis and chemical structures of the modified POSS.

POSS nanocomposites. The use of functionalized POSS moieties allows well-distributed nanosized POSS domains to be generated within polymer matrices; they can also function as physical crosslinking sites.[7–9] On the other hand, larger aggregated POSS domains can behave as conventional fillers that might degrade the physical properties of the polymer matrix.[24–29] Because of their porous nature, POSS units possess low dielectric constants[30–34]; therefore, POSS-containing polyimide composites will have low dielectric constants and good mechanical and thermal properties if their POSS units are distributed evenly and adhered well to the polyimide matrix. Although chemically attaching POSS units to the polyimide matrix has been the approach generally used, complicated chemical reactions are involved.[28,29] Physical blending is the convenient alternative toward obtaining the desired composites; the compatibility of the components is the most important criterion affecting the morphologies and properties of the resultant blends. In this study, we synthesized a fluorinated functional POSS derivative that acts as a proton acceptor that forms hydrogen bonds with the polyimide matrix; this blend exhibits improved compatibility of its POSS derivative and polyimide components.

EXPERIMENTAL

Materials and Sample Preparation

Pyromellitic dianhydride (PMDA) was purchased from TCI (Tokyo, Japan) and used as received. Octakis(dimethylsilyloxy)silsesquioxane[$(HMe_2SiOSiO_{1.5})_8$], platinum 1,3-divinyl-1,1,3,3-tetramethyldisiloxane [Pt(dvs)], allyl propyl ether (APE), and 4,4-oxydianiline (ODA) were purchased from Aldrich (US) and used as received. Allyl 1,1,2,3,3,3-hexafluoropropyl ether (AHFPE) was obtained from Lancaster (US) and used as received. *N*,*N*-Dimethylacetamide (DMAc) was dried over P_2O_5 for 2 days and then distilled before use.

Synthesis of Multifunctional POSS

Two multifunctional POSS derivatives, one containing eight fluorinated ether groups [octakis (dimethylsiloxyhexafluoropropyl) silsesquioxane (OF)] and the other eight ether groups [octakis (dimethylsiloxypropyl) silsesquioxane (OP)], were synthesized as described previously (Scheme 1).[32–35] OF were prepared by the placement of (HMe2-$SiOSiO_{1.5})_8$ (0.5 g, 0.49 mmol) in a magnetically

stirred, 25-mL Schlenk flask and the addition of toluene (5 mL); the solution was stirred for 5 min. AHFPE (0.62 mL, 3.92 mmol) and then 10 drops of 2.0 mM Pt(dvs) were added. The mixture was stirred for 8 h at 80 °C. The mixture was cooled, and dry, activated charcoal was added. After it had been stirred for 10 min, the mixture was filtered through a 0.45-μm Teflon membrane into a vial and stored as 10 wt % clear solution. Removing the solvents yielded 1.05 g of an opaque, viscous liquid. OP was synthesized by the reaction of $Q_8M_8^H$ with an excess of APE. Purification steps of these mixtures are the same as earlier.

OF: ^{1}H NMR(500 MHz, [D_1]$CDCl_3$, 25 °C)): δ = 0.14 [$(CH_3)_2Si$], 0.6 (CH_2Si), 0.95 (CH_3CH), 1.38 (CH_3CHSi), 1.7 (CCH_2C), 3.92 (CH2O), 4.7, 4.8 (CHF); IR (KBr): ν = 1201 (CF_2), 1097 (Si—O—Si, POSS), 738 (CHF), 702 (CF_3) cm^{-1}.

OP: ^{1}H NMR(500 MHz, [D_1]$CDCl_3$, 25 °C)): δ = 0.18 [$(CH_3)_2Si$], 0.57 (CH_2Si), 1.57 (CCH_2C), 3.34 (CH_2O); IR (KBr): 1732 (—O—), 1100 (Si—O—Si, POSS) cm^{-1}.

Preparation of PI-POSS Nanocomposites

PAA solutions (PMDA-ODA) were prepared with the following steps: 10.00 mmol of ODA was fed into a three-necked flask that contained 25 g of DMAc with nitrogen purging at 25 °C. After ODA had dissolved, 10.20 mmol of PMDA was divided into three batches and added to the flask batch by batch at intervals of 0.5 h between batches. When PMDA had completely dissolved in the solution, the solution was stirred continuously for 1 h, yielding a viscous PAA solution. The final PAA content in DMAc was 15 wt %. Various mole fractions of the modified POSS (OF and OP) were stirred in the PAA solution for 24 h at room temperature, cast onto a glass slide using a doctor's blade, and then placed in a vacuum oven at 40 °C for 48 h. These PAA/POSS-modified mixtures were then imidized by placing them in an air circulation oven, heating first at 100, 150, 200, and 250 °C for 1 h each and then at 300 °C for 5 h to ensure complete imidization.

Characterization

FTIR spectra were recorded on a Nicolet Avatar 320 FTIR spectrophotometer from 4000 cm^{-1} to 400 cm^{-1} at a resolution of 1.0 cm^{-1} under a continuous flow of nitrogen. ^{1}H NMR spectra was recorded at 25 °C on an INOVA 500 MHz NMR spectrometer. Elemental analysis of the nanocomposites was performed using a Perkin-Elmer 2400 CHN analyzer. A DuPont Q100 thermogravimetric analyzer (TGA) was used to investigate the thermal stability of the nanocomposites; the samples (~10 mg) were heated from ambient temperature to 850 °C under a nitrogen atmosphere at a heating rate of 20 °C/min. Dynamic mechanical analyses were performed using a DuPont Q800 dynamic mechanical analyzer (DMA) over the temperature range 150–500 °C using a frequency of 1.0 Hz and a heating rate of 5 °C/min; data acquisition and analysis of the storage modulus (E') and loss tangent (tan δ) were performed automatically by the system using samples having a length of 14 mm, a width of 5 mm, and a thickness of 0.2 mm. Wide-angle X-ray scattering (WAXS) measurements were performed using a BL17A1 wiggler beamline at the National Synchrotron Radiation Research Center (NSRRC), Taiwan. To observe the morphology of the PI-POSS nanocomposites, the samples were fractured cryogenically using liquid nitrogen. Field scanning electronic microscopy (FE-SEM) images were obtained using a Hitachi-S4200 microscope operated at an acceleration voltage of 15 kV. The dielectric constant and dielectric loss were determined using a Du Pont 2970 dielectric analyzer (DEA) over the temperature range from 25 to 50 °C at a heating rate of 1 °C/min with scan frequencies ranging from 1 to 10^5 Hz. The measured densities (d^M) of polyimide nanocomposites films were obtained by dividing the weight of the films by their volume. The fractional free volume (FFV) was calculated from eq 1:

$$\mathrm{FFV} = (V_{sp} - 1.3V_w)/V_{sp} \quad (1)$$

where V_{sp} is the polymer bulk specific volume and V_w is the van der Waals volume.[36,37]

RESULTS AND DISCUSSION

Wide-Angle X-ray Scattering

The distribution of POSS domains within polymer matrices is an important factor dictating the final thermal and mechanical properties of the resulting composites. For the physical blending of polymers with POSS particles without covalent bonding, the compatibility between the components has a major effect on the final structure. For example, if the compatibility is poor, the aggregation or crystallization of POSS moieties usually

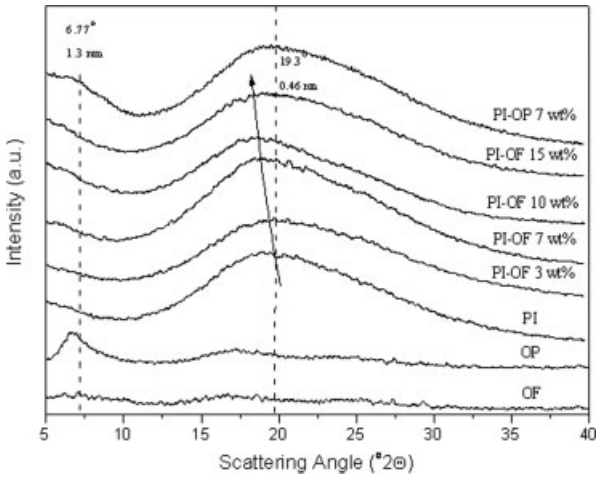

Figure 1. WAXS profiles of the modified POSS and the PI-POSS nanocomposites.

occurs within the polymer matrices. Figure 1 indicates that all of these composites provided only broad amorphous maxima because the polyimide and our two modified POSS polyimides were amorphous. We note that the amorphous peak of the pure polyimide ($2\theta = \sim 19.3^{\circ}$) shifted to a slightly lower value upon increasing the OF content: an indication of increasingly higher d spacings. In contrast, the amorphous maximum for the PI-OP composite remained essentially the same as that of the mother polyimide, implying that the spacing effect was insignificant in this system. Therefore, we suspected that the well-dispersed OF molecules separated the polyimide chain segments better than the OP molecules, causing the amorphous peak of the PI-OF composite to shift to a lower 2θ angle.

Morphologies

Figure 2 (a–f) present FE-SEM micrographs of the fractured surfaces of the PAA-POSS and PI-POSS nanocomposites. Both blends, PAA-OF and PAA-OP, were soluble at 15 wt % in DMAc. After evaporation of the solvent, the PAA-OF (15 wt % OF) blend remained miscible, exhibiting a single phase [Fig. 2(a)] as a result of the presence of hydrogen bonding interactions between PAA and OF. On the other hand, aggregated OP domains are clearly visible in the micrograph [Fig. 2(b)] of the PAA-OP (15 wt % OP) blend after evaporation of the solvent, presumably because of poorer hydrogen bonding interactions. Figure 2(c,e) reveals that relatively smaller sized OF particles (<30 mm) were evenly embedded within the polyimide matrix after imidization, implying that the miscible PAA-OF blend became an immiscible PI-OF blend, presumably because the decrease in the strength of the hydrogen bonding interactions during the imidization process lowers the enthalpic content of the free energy of mixing. It is interesting that the OF particle size remained almost unchanged upon changing the OF content from 3 to 15 wt %. The content of phase-separated OP in PAA-OP [15 wt % OP, Fig. 2(b)] was substantially lower than that in PI-OP [15 wt % OP, Fig. 2(f)], indicating that the PAA-OP blend was partially miscible with a significant fraction of OP dissolved in the PAA phase. The OF particles were relatively smaller and distributed more evenly in the PI-OF composites than were the OP particles in the PI-OP composites. In addition, the OP particles tended to interconnect in the PI-OP composite, whereas the OF particles were well separated in the PI-OF composite.

Fourier Transform Infrared (FTIR) Spectra

The FTIR spectra in Figure 3 indicate that the signal for the PAA amide groups at 1655 cm^{-1} shifted to higher wavenumber upon adding OF, implying that a fraction of the intramolecular hydrogen bonds of PAA (*N*—H···O=C and O—H···O=C) transformed into intermolecular interactions between the PAA and OF (e.g., O—H···F—C or *N*—H···F—C). In contrast, this signal did not change upon blending with OP, where intermolecular hydrogen bonding was not expected. In addition, hydrogen bonding between the siloxane units of OF and the OH and NH groups of PAA might also contribute to the enhanced compatibility between PAA and OF. We observe that the signal for the siloxane groups (Si—O—Si) at ~1100 cm^{-1} in PAA-OF broadens and shifts to lower wavenumber than that of the PAA-OP (Fig. 3). In previous studies,[38,39] we demonstrated the existence of hydrogen bonding interactions between the hydroxyl groups of amide and the siloxane units of POSS derivatives.

Phase Separation Mechanisms

Based on the FTIR spectra and morphological observations described earlier, in Scheme 2 we illustrate the possible phase separation mechanisms that occur during the solvent removal and thermal imidization processes for these two systems. During solvent evaporation, the PAA chains will pack increasingly closer together as a consequence of a concentration effect. At the end of the

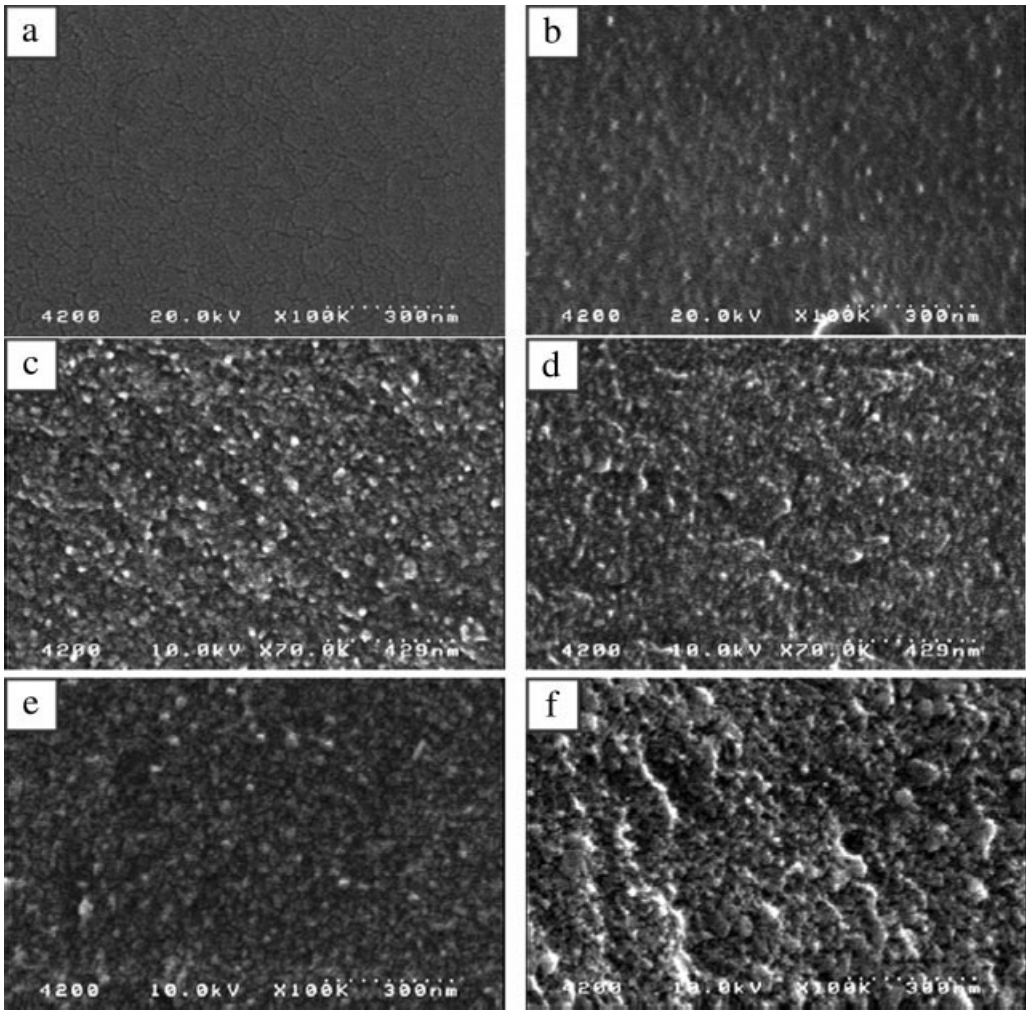

Figure 2. FE-SEM micrographs of the PAA-POSS and PI-POSS nanocomposites: (a) PAA-OF 15 wt %; (b) PAA-OP 15 wt %; (c) PI-OF 3 wt %; (d) PI-OP 3 wt %; (e) PI-OF 15 wt %; (f) PI-OP 15 wt %.

solvent removal process, the OF particles remained miscible with PAA to form a single-phase PAA-OF composite [Fig. 2(a)], whereas a fraction of the OP particles had separated and aggregated to form its own domains [Fig. 2(b)]. During the imidization process, where PAA gradually converted into the polyimide, the extent of hydrogen bonding between PAA and OF decreased gradually as a result of the gradual loss of proton donors. Because polyimide and OF are thermodynamically immiscible, phase separation and aggregation gradually occurred from the homogeneous PAA-OF mixture to form OF-only domains. In the partially miscible PAA-OP mixture, where only weak hydrogen bonds existed, the extent of OP phase separation and aggregation increased during the imidization process because polyimide and OP are immiscible. When the imidization was complete, the domain sizes of the OP aggregates were relatively larger than those of the OF aggregates. We suggest that the smaller domain sizes for OF result because it is more miscible with PI than OP.

Thermal Properties

Figures 4 and 5 display the glass transition temperatures (T_g) and the thermal stabilities, respectively, of the PI-POSS nanocomposites as measured using DMA and TGA, respectively. The value of T_g of the pure polyimide was 365.7 °C. The incorporation of OF particles resulted in a slight increase in T_g, whereas the addition of OP resulted in slight decrease. The incorporation of

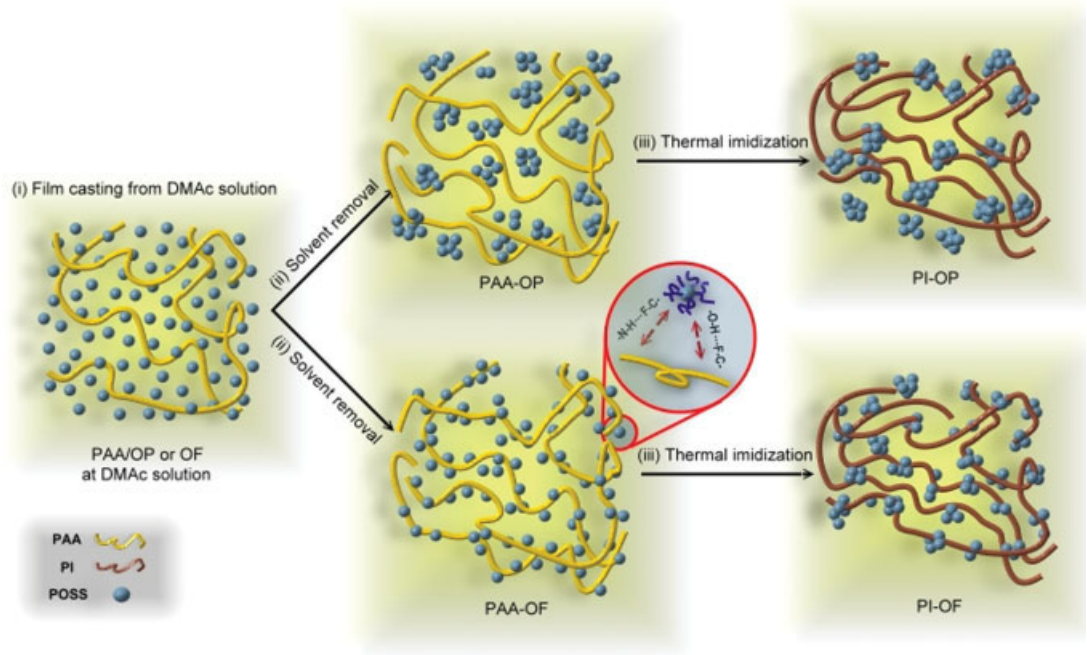

Scheme 2. Schematic representation of the deformation processes occurring during the imidization processes.

POSS moieties into polymer matrices, especially in miscible systems, can have two competitive and opposing effects on the value of T_g.[24–27,40–43] The rigid and bulky POSS unit tends to preclude close contact with surrounding polymer matrix chains and, thus, creates a greater void volume (or free volume) around the POSS units of the composite. A greater free volume generally favors a lower value of T_g for a polymer matrix. In contrast, the rigid and bulky structure of the POSS moiety tends to hinder chain movement, which generally leads to higher values of T_g. Table 1 indicates that the measured densities of the PI-OF and PI-OP composites were lower than those expected theoretically, implying that the precluding phenomenon was in effect. In terms of its lower density, the PI-OF system possessed a relatively higher free volume than did the PI-OP system at the same POSS content. We would, therefore, expect PI-OP to have a higher value of T_g than PI-OF if free volume were the only influencing factor. Table 1 indicates, however, that the opposite was true. Therefore, we believe that the hindrance of chain movement in PI-OF plays a more important role than does the free volume in dictating the ultimate value of T_g. The fluorine atoms in the OF macromolecules presumably interact with the polyimide through weak hydrogen bonding, which hinders chain motion and enhances T_g. In addition, these interactions help to create a physically cross-linked network surrounding the POSS particles and, thus, generate a greater free volume. The different trends of storage modulus properties between PI-OF and PI-OP nanocomposites also verified the effect of physical cross-linked network of OF in the polyimide matrix. The modulus in a rubbery state in the case of PI-OF when compared with polyimide reveals formation of physical cross-links composed of OF domains interacting with the polymer chain. On the contrary, modulus decreases in the PI-OP system because of the absence of such an interaction and POSS domains only dilute the system.

Figure 5 and Table 1 present the thermal stabilities of the various systems under nitrogen, as determined from the TGA thermograms. We chose the 5% mass loss temperatures ($T_{5\%}$) as a measure of the relative thermal stabilities of these composites. The value of $T_{5\%}$ of the PI-OP nanocomposite decreased considerably upon increasing of OP content because of the lower decomposition temperature of the low-molecular-weight OP. The value of $T_{5\%}$ of the PI-OF nanocomposite at up to 10 wt % OF remained almost unchanged relative to that of the pure polyimide, but it decreased significantly when the OF content was 15 wt %. It appears that the formation of a physically cross-linked network through weak

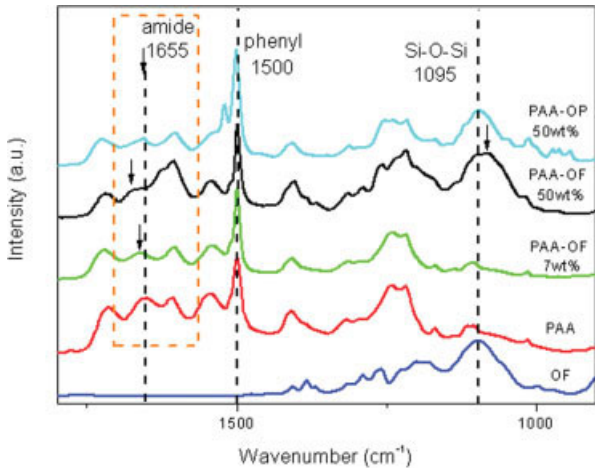

Figure 3. FTIR spectra of PAA and the PAA-POSS nanocomposites. [Color figure can be viewed in the online issue, which is available at www.interscience.wiley.com.]

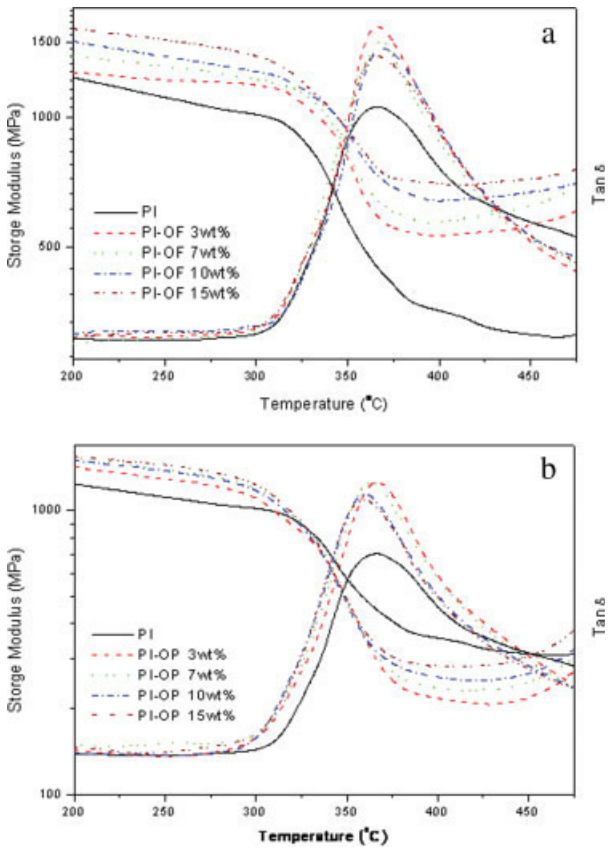

Figure 4. Dynamic shear storage modulus and loss factor tan δ of the (a) PI-OF and (b) PI-OP nanocomposites. [Color figure can be viewed in the online issue, which is available at www.interscience.wiley.com.]

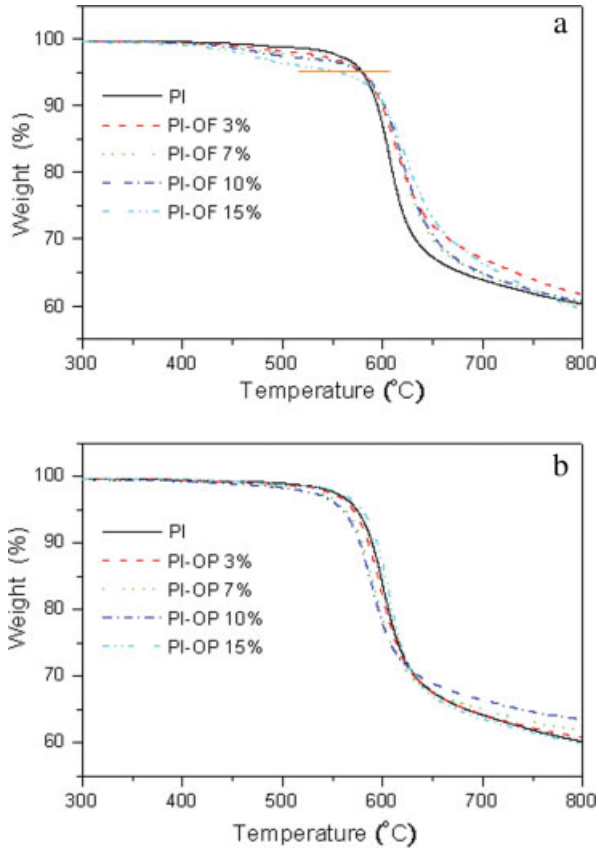

Figure 5. TGA curves for the (a) PI-OF and (b) PI-OP nanocomposites. [Color figure can be viewed in the online issue, which is available at www.interscience.wiley.com.]

hydrogen bonding decreased the volatility and decomposition of the low-molecular-weight OF in the PI-OF composites incorporating up to 10 wt % OF.

Porosity Versus Dielectric Constant

Table 1 summarizes the free volumes and dielectric constants (k) of the PI-OF and PI-OP nanocomposites. The incorporation of OF into the polyimide resulted in a gradual decrease of the dielectric constant from 3.19 (OF = 0 wt %) to 2.12 (OF = 15 wt %). We observed a similar trend for the PI-OP composites, except that the value of k decreased relatively slower than that of the PI-OF composites at the same loading of the POSS derivative. Presumably, the modified POSS reduce the dielectric constant of polyimide mainly through the increased porosity resulting from the presence of the POSS particles.

The porosity (void or free volume) of the PI-POSS nanocomposites arises from two

Table 1. Thermal Stability, Free Volume, and Thermomechanical and Dielectric Properties of PI-OF and PI-OP Nanocomposites.

Sample	T_g (°C)[a]	$T_{5\%}$ (°C)[b]	Dielectric Constant (at 100 kHz)	Dielectric Constant Decrease (Δk)	Theoretical Density (g/cm^3)[c]	Measured Density (g/cm^3)	Total Fractional Free Volume[d]	Free Volume Increase (Δf)
PI	366	578	3.19 ± 0.04	—	1.420	1.42 ± 0.03	0.048	—
PI-OP 3 wt %	366	574	2.87 ± 0.07	−0.32	1.411	1.37 ± 0.05	0.051	0.003
PI-OP 7 wt %	363	570	2.76 ± 0.09	−0.43	1.403	1.33 ± 0.04	0.081	0.033
PI-OP 10 wt %	360	563	2.65 ± 0.06	−0.54	1.397	1.30 ± 0.05	0.103	0.055
PI-OP 15 wt %	359	559	2.58 ± 0.06	−0.61	1.386	1.25 ± 0.06	0.140	0.092
PI-OF 3 wt %	369	578	2.72 ± 0.07	−0.47	1.408	1.36 ± 0.04	0.072	0.024
PI-OF 7 wt %	368	578	2.54 ± 0.05	−0.65	1.396	1.32 ± 0.06	0.114	0.066
PI-OF 10 wt %	371	578	2.33 ± 0.06	−0.86	1.390	1.27 ± 0.04	0.156	0.108
PI-OF 15 wt %	369	553	2.12 ± 0.08	−1.07	1.376	1.21 ± 0.05	0.212	0.164

[a] T_g is the temperature of the maximum of the loss factor tan δ.
[b] $T_{5\%}$ are the temperatures corresponding to five losses of mass, respectively, under N_2.
[c] Densities of OP, OF, and the pure polyimide were about 1.23, 1.17, and 1.42 g/cm^3, respectively.
[d] Total free volume fractional calculated using Bondi and Freeman's method.[36,37]

phenomena: (1) the intrinsic nanoporosity of the POSS core and (2) the exclusion effect caused by the bulky and rigid POSS cage. The porosities induced by the POSS cores should be identical for the PI-OF and PI-OP nanocomposites at the same POSS content. As mentioned earlier, the greater void volume surrounding the POSS units in PI-OF, relative to that in PI-OP, was probably due to the presence of stronger noncovalent interactions and/or the formation of a weak physically cross-linked network structure surrounding the POSS core in the former system. The porosity of a sample can be expressed in terms of the free volume, which can be measured from its density. Figure 6 displays a plot of the change in dielectric constant ($-\Delta k$) as a function of the change in free volume (Δf), using the virgin polyimide as the reference sample. We note that the value of k decreased almost linearly upon increasing the free volume for both the PI-OF and PI-OP nanocomposites. The PI-OF nanocomposite exhibited a more efficient reduction in its dielectric constant than did the PI-OF system at the same free volume content. It appears that the presence of fluorine atoms in the PI-OF system also contributed to the lower dielectric constant of the composite.

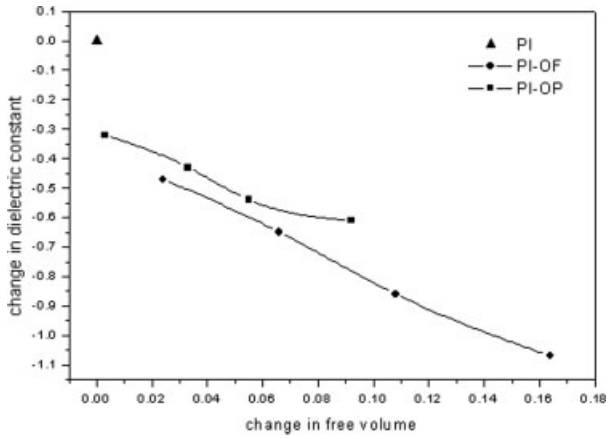

Figure 6. Plot of the change in dielectric constant as a function of the change in free volume.

CONCLUSIONS

We prepared fluoropropyl- and propyl-functionalized POSS derivatives through hydrosilylation. The fluorine-functionalized POSS derivative blended with PAA produced a high-performance polyimide nanocomposite exhibiting an extremely low dielectric constant. The existence of effective intermolecular interactions between PAA and OF increased their compatibility, resulting in better dispersion of these POSS cages within the polyimide matrix and improved thermal and dielectric properties for the PI-OF nanocomposites relative to the PI-OP system. For the PI-OF nanocomposites, a combination of the intrinsic porosity of the POSS cage, the stronger hydrogen bonding interactions, the greater free volume, and the lower polarizability of the fluorine-containing POSS was responsible for the observed extremely low dielectric constant. This article presents a simple and efficient method for preparing polyimide

nanocomposites with low dielectric constants and good thermal properties: simply blending the polyimide precursor with the fluorine-containing POSS derivative OF.

REFERENCES AND NOTES

1. Hougham, G.; Tesoro, G.; Shaw, J. Macromolecules 1994, 27, 3642–3649.
2. Park, S. J.; Cho, K. S.; Kim, S. H. J Colloid Interface Sci 2004, 272, 384–390.
3. Hougham, G.; Tesoro, G.; Viehbeck, A. Macromolecules 1996, 29, 3453–3456.
4. Chung, I. S.; Park, C. E.; Ree, M. S.; Kim, Y. Chem Mater 2001, 13, 2801–2806.
5. Onah, E. J. Chem Mater 2003, 15, 4104.
6. Sasaki, S.; Nishi, S. In Synthesis of Fluorinated Polyimides; Ghosh, M. K.; Mittal, K. L., Eds.; Marcel Dekker: New York, 1996; pp 71–120.
7. Hedrick, J. L.; Carter, K. R.; Richter, R.; Miller, R. D.; Russell, T. P.; Flores, V. Chem Mater 1998, 10, 39–49.
8. Carter, K. R.; DiPietro, R. A.; Sanchez, M. I.; Swanson, S. A. Chem Mater 2001, 13, 213–221.
9. Michael, S. S.; Michal, S. C.; Barry, J. B.; Ronald, C. H.; Lee, H. J.; Brian, G. L. Macromolecules 2005, 38, 4301–4310.
10. Fu, G. D.; Zong, B. Y.; Kang, E. T.; Neoh, K. G.; Lin, C. C.; Liaw, D. J. Ind Eng Chem Res 2004, 43, 6723–6730.
11. Silicon-Containing Polymers; Jones, R. G.; Ando, W. J. C., Eds.; Springer-Verlag: New York 2000.
12. Seino, M. T.; Hayakawa, Y.; Inhida, M.; Kakimoto, K.; Watanabe, H. O. Macromolecules 2006, 39, 3473–3475.
13. Zucchi, I. A.; Galante, M. J. R.; Williams, J. J.; Franchini, E.; Galy, J.; Gérard, J. F. Macromolecules 2007, 40, 1274–1282.
14. Voronkov, M. G.; Lavrent'ev, V. I. Top Curr Chem 1982, 102, 119–236.
15. Baney, R. H.; Itoh, M.; Sakakibara, A.; Suzuki, T. Chem Rev 1995, 95, 1409–1430.
16. Provatas, J. G. Trends Polym Sci 1997, 5, 327–332.
17. Loy, D. A.; Shea, K. J. Chem Rev 1995, 95, 1431–1432.
18. Lichtenhan, Vol. 10; Salmone, J. C., Ed.; CRC Press: New York, 1996; pp 7768–7777.
19. Laine, R. M. J Mater Chem 2005, 15, 44–52.
20. Xu, H.; Yang, B.; Wang, J.; Guang, S.; Li, C. J Polym Sci Part A: Polym Chem 2007, 45, 5308–5317.
21. Mariani, A.; Alzari, V.; Monticelli, O. J Polym Sci Part A: Polym Chem 2007, 45, 4514–4521.
22. Amir, N.; Levina, A.; Silverstein, M. S. J Polym Sci Part A: Polym Chem 2007, 45, 4264–4268.
23. Liu, Y. L.; Chang, G. P.; Hsu, K. Y.; Chang, F. C. J Polym Sci Part A: Polym Chem 2006, 44, 3825–3830.
24. Strachota, A.; Kroutilová, I.; Kovářová, J.; Matějka, L. Macromolecules 2004, 37, 9457–9464.
25. Ni, Y.; Zheng, S.; Nie, K. Polymer 2004, 45, 5557–5568.
26. Liu, Y. L.; Lee, H. C. J Polym Sci Part A: Polym Chem 2006, 44, 4632–4643.
27. Liu, H.; Zheng, S.; Nie, K. Macromolecules 2005, 38, 5088–5097.
28. Zhang, C.; Babonneau, F.; Bonhomme, C.; Laine, R. M.; Soles, C. L.; Hristov, H. A.; Yee, A. F. J Am Chem Soc 1998, 120, 8380–8391.
29. Wu, S.; Hayakawa, T.; Kikuchi, R.; Grunzinger, S. J.; Kakimoto, M. Macromolecules 2007, 40, 5698–5705.
30. Leu, C. M.; Chang, Y. T.; Wei, K. H. Chem Mater 2003, 15, 3721–3727.
31. Leu, C. M.; Chang, Y. T.; Wei, K. H. Chem Mater 2003, 15, 2261–2265.
32. Lee, Y. J.; Huang, J. M.; Kuo, S. W.; Lu, J. S.; Chang, F. C. Polymer 2005, 46, 173–181.
33. Lee, Y. J.; Huang, J. M.; Kuo, S. W.; Chang, F. C. Polymer 2005, 46, 10056–10065.
34. Ye, Y. S.; Chen, W. Y.; Wang, Y. Z. J Polym Sci Part A: Polym Chem 2006, 44, 5391–5395.
35. Chen, W. Y.; Ko, S. H.; Hsieh, T. H.; Chang, F. C.; Wang, Y. Z. Macromol Rapid Commun 2006, 27, 452–457.
36. Bondi, A. J Phys Chem 1964, 68, 441–453.
37. Freeman, B. D.; Hill, A. J. In Structure and Properties of Glassy Polymers; Tant, M. R.; Hill, A. J., Eds.; American Chem society: Washington, D. C., 1998; pp 306–325.
38. Lin, H. M.; Wu, S. Y.; Huang, P. Y.; Huang, C. F.; Kuo, S. W.; Chang, F. C. Macromol Rapid Commun 2006, 27, 1550–1555.
39. Huang, C. F.; Kuo, S. W.; Lin, F. J.; Huang, W. J.; Wang, C. F.; Chen, W. Y.; Chang, F. C. Macromolecules 2006, 39, 300–308.
40. Xu, H.; Kuo, S. W.; Lee, J. S.; Chang, F. C. Polymer 2002, 43, 5117–5124.
41. Yen, Y. C.; Ye, Y. S.; Cheng, C. C.; Chen, H. M.; Sheu, H. S.; Chang, F. C. Polymer 2008, doi: 10.1016/j.polymer.2005.06.025
42. Romo-Uribe, A.; Mather, P. T.; Haddad, T. S.; Lichtenhan, J. D. J Polym. Sci Part B: Polym Phys 1998, 36, 1857–1872.
43. Bharadwaj, R. K.; Berry, R. J.; Farmer, B. L. Polymer 2000, 41, 7209–7255.